Journal of Biomolecular NMR (2023) 77:121–130
https://doi.org/10.1007/s10858-023-00416-5

ARTICLE

Efficient 18.8 T MAS-DNP NMR reveals hidden side chains in amyloid fibrils

Alons Lends[1] · Nicolas Birlirakis[2] · Xinyi Cai[3] · Asen Daskalov[1] · Jayakrishna Shenoy[1] · Muhammed Bilal Abdul-Shukkoor[1] · Mélanie Berbon[1] · Fabien Ferrage[2] · Yangping Liu[3] · Antoine Loquet[1] · Kong Ooi Tan[2]

Received: 4 January 2023 / Accepted: 2 May 2023 / Published online: 8 June 2023

Abstract

Amyloid fibrils are large and insoluble protein assemblies composed of a rigid core associated with a cross-β arrangement rich in β-sheet structural elements. It has been widely observed in solid-state NMR experiments that semi-rigid protein segments or side chains do not yield easily observable NMR signals at room temperature. The reasons for the missing peaks may be due to the presence of unfavorable dynamics that interfere with NMR experiments, which result in very weak or unobservable NMR signals. Therefore, for amyloid fibrils, semi-rigid and dynamically disordered segments flanking the amyloid core are very challenging to study. Here, we show that high-field dynamic nuclear polarization (DNP), an NMR hyperpolarization technique typically performed at low temperatures, can circumvent this issue because (i) the low-temperature environment (~ 100 K) slows down the protein dynamics to escape unfavorable detection regime, (ii) DNP improves the overall NMR sensitivity including those of flexible side chains, and (iii) efficient cross-effect DNP biradicals (SNAPol-1) optimized for high-field DNP (≥ 18.8 T) are employed to offer high sensitivity and resolution suitable for biomolecular NMR applications. By combining these factors, we have successfully established an impressive enhancement factor of $\varepsilon \sim 50$ on amyloid fibrils using an 18.8 T/ 800 MHz magnet. We have compared the DNP efficiencies of M-TinyPol, NATriPol-3, and SNAPol-1 biradicals on amyloid fibrils. We found that SNAPol-1 (with $\varepsilon \sim 50$) outperformed the other two radicals. The MAS DNP experiments revealed signals of flexible side chains previously inaccessible at conventional room-temperature experiments. These results demonstrate the potential of MAS-DNP NMR as a valuable tool for structural investigations of amyloid fibrils, particularly for side chains and dynamically disordered segments otherwise hidden at room temperature.

Keywords Amyloid fibrils · Solid-state NMR · Dynamic nuclear polarization

Introduction

Amyloid fibrils are self-assembled protein aggregates that have been associated with numerous human disorders, including Alzheimer's and Parkinson's diseases (Ke et al. 2020; Dobson et al. 2020). On the other hand, some amyloid fibrils play important roles in certain physiological functions (i.e. functional amyloids) (Loquet et al. 2018a). For instance, functional amyloids play essential roles in hormone storage (Maji et al. 2009), bacterial curli formations (Chapman et al. 2002), or in regulated cell death mechanisms in fungi (Chapman et al. 2002; Loquet and Saupe 2017). Their 3D structures are crucial for elucidating the structure–function relationship of these systems at the molecular level. For example, the triangular beta-solenoid amyloid fold uncovered by solid-state NMR (ssNMR) in the fungal amyloid

✉ Antoine Loquet
a.loquet@iecb.u-bordeaux.fr

✉ Kong Ooi Tan
kong-ooi.tan@ens.psl.eu

[1] CNRS, Chemistry and Biology of Membranes and Nanoobjects (CBMN), UMR 5348, Institut Europeen de Chimie et Biologie (IECB), University of Bordeaux, 33600 Pessac, France

[2] Laboratoire des Biomolécules, LBM, Département de Chimie, École Normale Supérieure, PSL University, Sorbonne Université, CNRS, 75005 Paris, France

[3] Tianjin Key Laboratory on Technologies Enabling Development of Clinical Therapeutics and Diagnostics, School of Pharmacy, Tianjin Medical University, Tianjin 300070, China

fibrils of HET-s (Wasmer et al. 2008) and HELLF (Daskalov et al. 2020) was demonstrated to be essential for amyloid cross-seeding and required to trigger a regulated cell death reaction in filamentous fungi (Daskalov et al. 2020). Due to their insolubility and lack of a crystalline order, amyloid fibrils still constitute very challenging targets for structural biology. Additionally, they often exhibit a remarkable degree of local structural polymorphism (Tycko 2014). High-resolution 3D structures of amyloid fibrils can be experimentally accessed by cryo-electron microscopy (cryo-EM) (Fitzpatrick and Saibil 2019) and magic-angle spinning (MAS) NMR (Daskalov et al. 2021; Meier and Böckmann 2015; Wel 2017; Jaroniec 2019). In contrast to cryo-EM, ssNMR techniques provide access to atomic-level information on dynamics at different times scales and site-specific polymorphism (Siemer 2020). However, one of the main disadvantages of ssNMR is its inherently low sensitivity, often leading to long measurement times to perform multidimensional experiments required for extracting distance restraints required for structure determination (Loquet et al. 2018b). The sensitivity issue can be circumvented by employing dynamic nuclear polarization (DNP) (Su et al. 2015; Biedenbänder et al. 2022), which is an NMR hyperpolarization technique that mediates polarization transfer from unpaired electrons or radicals to nuclei via strategic microwave irradiation. In MAS DNP experiments, gyrotrons, high-frequency microwave sources capable of generating 20–100 W of microwaves, are employed to irradiate samples at low temperatures ($\leq$ 100 K) for efficient performances (Matsuki et al. 2016; Thurber et al. 2010; Li et al. 2021; Thurber and Tycko 2016; Sesti et al. 2018). To cryoprotect the precious biological NMR samples, glycerol- or trehalose-water mixtures are often used to homogeneously disperse the doped radicals across the amorphous sample (Takahashi et al. 2013). This hyperpolarization technique has paved the way for ssNMR to obtain important structural information on biosolids (including amyloid fibrils) (Jaudzems et al. 2019; Zhao et al. 2020; Maciejko et al. 2015; Marin-Montesinos et al. 2019; Gauto et al. 2021; Bayro et al. 2011; Debelouchina et al. 2013; Frederick et al. 2017; Lopez del Amo et al. 2013; Nagaraj 2016; Potapov et al. 2015; Deo et al. 2021) and inorganic materials that were previously inaccessible due to poor sensitivity (Rankin et al. 2019).

Although the theoretical maximum DNP enhancement factor ε is ~ 658 for ^{1}H nuclei, an actual experimental gain of up to 200 ~ 300 were reported in actual MAS DNP experiments performed at ~ 9 T and $\geq$ 80 K at 14.1 T (Mathies et al. 2015; Lilly Thankamony et al. 2017; Conroy et al. 2022; Akbey et al. 2012; Menzildjian et al. 2021) The development of higher-field DNP instruments at 18.8 T and 21.1 T is motivated by the fact that high-field NMR spectroscopy offers a better chemical-shift dispersion (Lund et al. 2020; Felch et al. 2013; Blank et al. 2016), i.e., it allows NMR peaks to be better resolved and constitutes a crucial aspect for biological NMR applications. However, it is known that the main MAS-DNP mechanism, cross effect, has decreasing DNP performance (or lower ε) with increasing magnetic field (Mathies et al. 2015; Tan et al. 2019a). Although pulsed DNP techniques with field-independent performances have been suggested to circumvent this issue (Henstra et al. 1988; Tan et al. 2019b; Wili et al. 2022; Redrouthu and Mathies 2022), their stringent microwave power requirement has limited experimental demonstrations to low fields ($\leq$ 1.2 T). An alternate strategy is to design a new class of DNP polarizing agents (or hetero-biradicals) that maximally exploit the cross-effect matching conditions at high magnetic fields (Mathies et al. 2015; Lund et al. 2020; Wisser et al. 2018; Berruyer et al. 2020; Halbritter et al. 2022) Among these novel biradicals, we will characterize the DNP performances of M-TinyPol, NATriPol-3, and SNAPol-1 radicals, which were demonstrated to yield efficient DNP performances (vide infra) (Zhai et al. 2020; Cai et al. 2021).

Molecular motions present in biological macromolecules average NMR interactions (such as chemical shifts) over different conformations and thus may lead to narrow lines. When such motions become frozen at low temperatures required for DNP experiments, the distribution of conformational states leads to significant inhomogeneous NMR line broadening or lower peak resolution (Bauer et al. 2017). However, it was reported in the literature such deleterious features are less severe for rigid biological molecules or small peptides (Fricke et al. 2014; Bahri et al. 2022; Gauto et al. 2019; Barnes et al. 2010; Barnes et al. 2009). For molecules exhibiting motions in the intermediate timescale, such as semi-rigid side chains of amino acids or mobile loop regions in proteins, it could be difficult to efficiently detect signals at room temperature using either dipolar- or *J*-based techniques (Ravotti et al. 2016; Colvin et al. 2015). This is because the dipolar couplings are too small (or well-averaged) for efficient cross-polarization (CP) transfer, while they could be still large enough to interfere with the coherences generated in the *J*-based Insensitive Nuclei Exchanged by Polarization Transfer (INEPT) (Ravotti et al. 2016; Colvin et al. 2015; Siemer et al. 2006; Heise et al. 2008; Jirasko et al. 2021; Ni et al. 2017; Gath et al. 2014; Wiegand et al. 2016; Björklund et al. 2013). Other possibilities that could make NMR peaks invisible include the interference between the dynamics of molecules with the MAS frequency and/or ^{1}H decoupling Rabi fields (Ni et al. 2017; Maus et al. 1996).

Observing these semi-rigid loops and side chains by MAS DNP measurements would allow a more accurate determination of their properties. For instance, it will be advantageous to extract additional distance restraints from residues that are mobile and hidden at room temperature—but become more rigid at lower temperatures—for structure calculations

(Jaudzems 2018). Lowering the temperatures to observe NMR peaks of these functionally important semi-rigid parts to slow down the deleterious intermediate dynamics coincidently improves DNP performances.

In this communication, we have performed MAS DNP experiments at a high magnetic field $B_0 = 18.8$ T (800 MHz ^{1}H Larmor frequency) using efficient hetero-biradical, SNAPol-1, to demonstrate unprecedented ^{13}C signal enhancement ε of ~ 50 for amyloid fibrils. These protein assemblies exhibit a sufficient spectral resolution in ^{13}C and ^{15}N dimensions at cryogenic temperature, enabling the observation of highly sensitive 2D ^{15}N-^{13}C correlation experiments using the PAIN-CP transfer scheme. Our results pave the way to develop DNP-enhanced ssNMR approaches using ^{15}N-^{13}C correlation experiments to reveal signals of semi-rigid side chain that are otherwise hidden at room temperature. In addition, the experiments reveal new peaks that allow the extraction of structural information on less rigid protein segments in protein assemblies.

Results and discussion

We prepared a ^{13}C, ^{15}N-labeled HET-s(218–289) protein sample, aggregated into amyloid fibrils with 5 mM M-TinyPol radical in DNP juice, which is a mixture of d_8-glycerol/D_2O/H_2O in a 6:3:1 by volume ratio. A DNP experiment was performed at 10 kHz MAS using a 3.2 mm sapphire rotor, temperature T ~ 100 K, and a magnetic field $B_0 = 18.8$ T (see Experimental Section for further details). The ^{1}H-^{13}C CP spectrum showed an enhancement ε ~ 10 (Fig. S1). We have doped the NWD2 fibrillar sample (Daskalov et al. 2015) with NATriPol-3 radical, which exhibited a similar performance as M-TinyPol (ε ~ 6) (see Fig. S2). Note that Bahri et al. have recently reported a DNP study on amyloid fibrils of $A\beta_{1\text{-}42}$ using the same radical (M-TinyPol) at the same magnetic field but with a faster spinning frequency of 40 kHz using a 1.3 mm rotor (Bahri et al. 2022), which yielded to a higher ε ~ 22, likely due to better microwave coupling, and, hence, higher electron Rabi field (Berruyer et al. 2020; Purea et al. 2019). Figure 1a shows a 2D ^{13}C DARR spectrum of DNP-enhanced HET-s amyloid fibrils. We observed ^{13}C linewidths for isolated peaks in the range of ~ 200–300 Hz. Note that the low-temperature DNP spectrum has 2–3 × broadened lines relative to the room-temperature spectrum (overlayed in Fig. 1a), which has reported linewidths for the same protein system of ~ 100 Hz (Siemer et al. 2005). The relatively moderate line broadening effect indicates a high structural homogeneity (or rigidity) of HET-s amyloid fibrils even at a temperature of 100 K. So far, the most narrow ^{13}C linewidths for amyloid fibrils at cryogenic temperatures have been reported for the $A\beta_{40}$ and $A\beta_{42}$ proteins (perspectives for DNP 2013; Bahri et al. 2022), implying that both of these proteins retain a sufficient homogeneity at low temperature. Note that ^{13}C linewidths as narrow as 30 Hz and 81 Hz could be achieved in amino acids and tripeptides, respectively, at cryogenic temperatures (Barnes et al. 2010; Barnes et al. 2009).

In our current study, we observed that ^{13}Cα/Cβ cross-peaks for alanine residues in the fibrils were not uniformly DNP-enhanced and do not have the same linewidths (see Fig. 1c). In particular, the Ala228 Cα/Cβ peak has weaker signal intensity, but narrower linewidth compared to the Ala237, Ala247, and Ala248 peaks. This can be explained by the fact that Ala228 is pointing inside the hydrophobic core of the triangular beta-solenoid fold of HETs (Fig. 1b), and, therefore, less accessible to the radical-doped solvent. On the contrary, the other Ala residues are in the disordered regions, which are much more exposed to the radical-doped solvent. Therefore, these alanine residues might be more efficiently enhanced while undergoing higher structural heterogeneity explaining the larger linewidths. The peaks were assigned based on assignments obtained from previously measured RT experiments. Here, we emphasize that the DNP experiments not only provide sensitivity enhancement, but are also useful in assessing solvent accessibility of local protein residues. Such an information is sometimes not directly obtainable using conventional NMR spectroscopy.

It is important to note that NMR linewidths in proteins under MAS depend on multiple factors, i.e., magnetic field strength, MAS frequency, processing parameters, radical concentration, and site-specific hydration (Bauer et al. 2017; Jaudzems 2018; David et al. 2018). To document these observations and compare our NMR data obtained on HET-s amyloid fibrils doped with NATriPol-3, we have compiled detailed ^{13}C linewidths of previously reported amyloid fibrils at low temperatures in Table 1. We note that the linewidths obtained in our experiments on HET-s are comparable to or even better than previously reported results in the literature.

HET-s in its fibrillar amyloid state forms a rigid β-solenoid spanning residues 226–246 (first repeat) and residues 262–282 (second repeat) (Melckebeke et al. 2010). In the DNP experiment, we observed additional ^{13}C–^{13}C correlations involving aromatic atoms (120–130 ppm spectral region in Fig. 1a) that were previously absent in the experiment recorded at room temperature.

To complement the observation of ^{13}C sites, we used multidimensional ^{15}N–^{13}C spectroscopy to access ^{15}N dimension. We have observed several cross peaks in the δ(^{13}C) ~ 140 ppm and δ(^{15}N) ~ 130 ppm region in Fig. 2 that corresponds to His residues. These His cross peaks could either be assigned to the 6-His residues from the His-tag at C-terminus of the sample, or His242 that is in the flexible loop region that connect the two beta-solenoid repeats. None of these His residues were previously observable in RT experiment. Thus, we have established an experimental

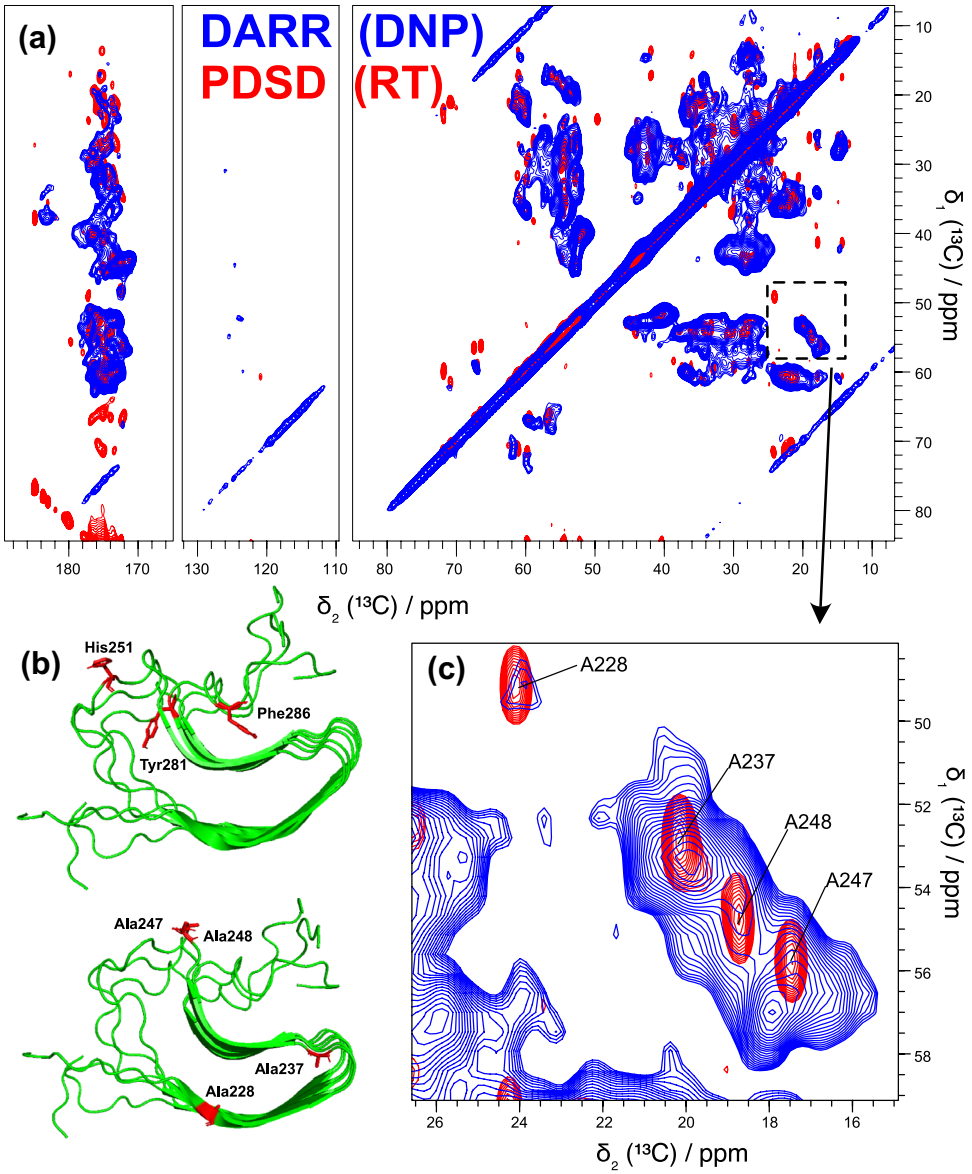

Fig. 1 **a** 2D ^{13}C-^{13}C 20 ms DARR spectrum of HET-s(218–289) amyloid fibrils recorded with DNP at 100 K (blue), overlayed with a 50 ms PDSD spectrum acquired at room temperature (red). **b** 3D structure of HET-s(218–289) amyloid fibrils (PDB entry 2rnm), with aromatic and alanine residues showed with a stick representation and colored in red, the image of protein was genererated using PyMOL. **c** Excerpt from Fig. 1a with a lower base contour level showing the Cβ/Cα spectral region or alanine residues of HET-s(218–289) amyloid fibrils

set up that could allow the detection of the His residues that are otherwise not detectable at room temperature. Further experiments (i.e., a 3D NCC correlation experiment) would be required to perform an unambiguous sequential assignment of these residues.

Notably, the ^{13}C linewidths for aromatic residues have broadened marginally from ~ 120 Hz to ~ 150 Hz between the room-temperature and low-temperature DNP experiments. This implies a relatively high structural homogeneity for otherwise mobile sidechains. The 2D NCa spectrum (Fig. 2) exhibited quite broad ^{15}N linewidths (~ 300 Hz), indicating that the ^{15}N nuclei could be more sensitive to structural inhomogeneity due to cryogenic temperatures. A similar feature has also been observed for microcrystalline proteins at low temperatures (Gauto et al. 2019; Jaudzems 2018).

Interestingly, the ^{15}N–^{13}C correlation DNP spectrum revealed new peaks at ^{15}N chemical shift below 100 ppm and ^{13}C chemical shift at ~ 107 and ~ 157 ppm (labelled in Fig. 2), which we assigned as ^{15}N side chain nuclei. By inspecting the reported Cα chemical shifts for the HET-s(218–289) protein at RT (Melckebeke et al. 2010), we have assigned these correlations and we established new N–C proximities, i.e., 236ArgNζ-Cδ, 274ArgNζ-Cδ, and 270LysNζ-Cε in the DNP spectrum (Fig. 2) that are helpful for sidechain assignment.

Next, we examined the DNP performance of using SNAPol-1, a trityl-nitroxide hetero-biradical that has recently demonstrated an ε ~ 110 on ubiquitin using a 3.2 mm DNP system at 18.8 T (Cai et al. 2021). We added 5 mM SNAPol-1 to ^{13}C, ^{15}N-labeled NWD2 amyloid fibrils, which share a similar beta-solenoid fold as observed in HET-s (Daskalov et al. 2015), and found that the SNAPol-1

Table 1 ^{13}C linewidths of different amyloid fibrils obtained at low temperatures reported in the literature

Sample	^{13}C linewidth	B_0 field (MHz)	Apodization	T (K)	References	Remarks
HETs(218–289)	0.96–1.5 ppm 192–305 Hz	800	Qsine 3	100	This study	Extracted from 8 isolated peaks
HETs(218–289)	1–2.5 ppm 150–375 Hz	600	Qsine 2.2	100	Bauer, JBioNMR, 2017	Low temperature only (no DNP), residue-dependent
PI3 K-SH3 fibrils	2–3 ppm 200–300 Hz	400	N.A	100	Bayro, JACS, 2011	
AB_{1-40}	0.7–0.8 ppm 140–160 Hz	850	N.A	100	Del Amo, JBioNMR, 2013	Low temperature only (no DNP)
AB_{1-40}, protofibrils	3.0 – 5.2 ppm 300–520 Hz	400	150 Hz Gaussian	25	Potapov, JACS, 2015	
AB_{1-40}, neutral pH	4.4 – 7.4 ppm 440–740 Hz	400	150 Hz Gaussian	25	Potapov, JACS, 2015	
AB_{1-40}, fibrils	2.4 – 3.2 ppm 240–320 Hz	400	150 Hz Gaussian	25	Potapov, JACS, 2015	
CsgA amyloid fibrils	2.7–4.3 ppm 270–430 Hz	400	N.A	110	Nagaraj, Chem-BioChem, 2016	Depends on the concentration of TOTAPOL radicals
AB_{1-42}	~0.6 ppm 120 Hz	800	QSine3	110	Bahri, PNAS 2022	

Data that is not available is denoted by N.A

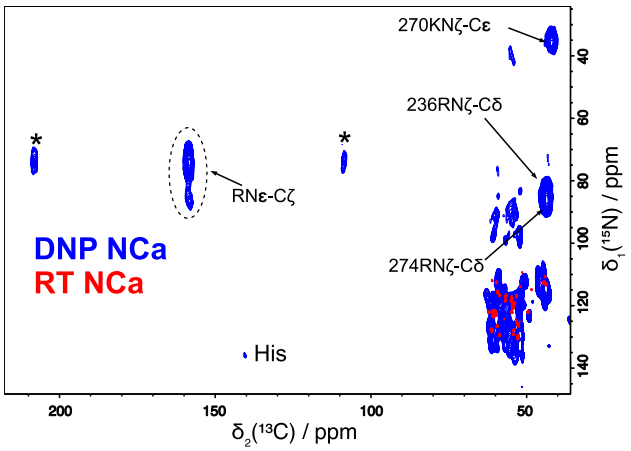

Fig. 2 2D ^{15}N–^{13}C NCa spectrum of HET-s(218–289) amyloid fibrils recorded with DNP at 100 K (blue), overlayed with spectrum recorded at room temperature (red). The * sign denotes the MAS spinning sidebands

sample yields a higher bulk ^{1}H enhancement (Fig. S3, ε ~ 22) than the NATriPol-3 sample (ε ~ 8). Following that, we obtained a highly promising enhancement of ε ~ 50 in a ^{1}H–^{13}C CP spectrum using SNAPol-1 at 11 kHz MAS frequency (Fig. 3a). Hence, we conclude that SNAPol-1 is a more efficient polarizing agent for DNP experiments on amyloid fibrils. Note that the high ε ~ 50 includes an additional 10% DNP improvement achieved by performing a freeze–pump–thaw procedure, which is a known procedure that removes dissolved paramagnetic oxygen that compromises the DNP samples (see Sample Preparation) (Delage-Laurin et al. 2021; Kubicki et al. 2014). To the best of our knowledge, ε ~ 50 is the highest DNP enhancement factor achieved for amyloid fibrils at 18.8 T reported to date. We anticipate that even more efficient DNP performance could be obtained for the 1.3 mm DNP system due to a more efficient microwave transmission system (or higher electron Rabi field) (Purea et al. 2019). Besides, the use of a smaller rotor with 4 × faster (~ 40 kHz) spinning frequency could lead to fewer spinning sidebands, less spectral overlap, and narrower linewidths. We also noted different enhancement factors were obtained between the simple ^{1}H direct pulse (ε ~ 22) (Fig. S3) and the CP experiment (ε ~ 50) (Fig. 3A). This is likely because that some ^{1}H nuclei in the sample are less accessible to the radical-doped DNP juice, i.e., hydrophobic residues in the core of the fibrils (vide supra) or the pools of bound water pools enclosed by the fibrils (Bauer et al. 2017; Melckebeke et al. 2011; Fitzpatrick et al. 2013). Moreover, we expect this feature to be sample and solvent dependent (Marin-Montesinos et al. 2019).

The excellent signal enhancement allowed us to observe new peaks in the DNP-NCa spectrum (Fig. 3b). Based on their chemical shifts, these new peaks could originate from the side chains. These peaks were not observed in conventional room-temperature ssNMR experiments, probably due to unfavorable dynamics that interfere with the timescale of dipolar-based experiments such as CP or ^{1}H-decoupling in MAS experiments. Based on studies reported in the literature, we speculate that the dynamics exhibited by these residues are likely to be in the 10^{3}–10^{6} s^{-1} (or μs) regime (Ni

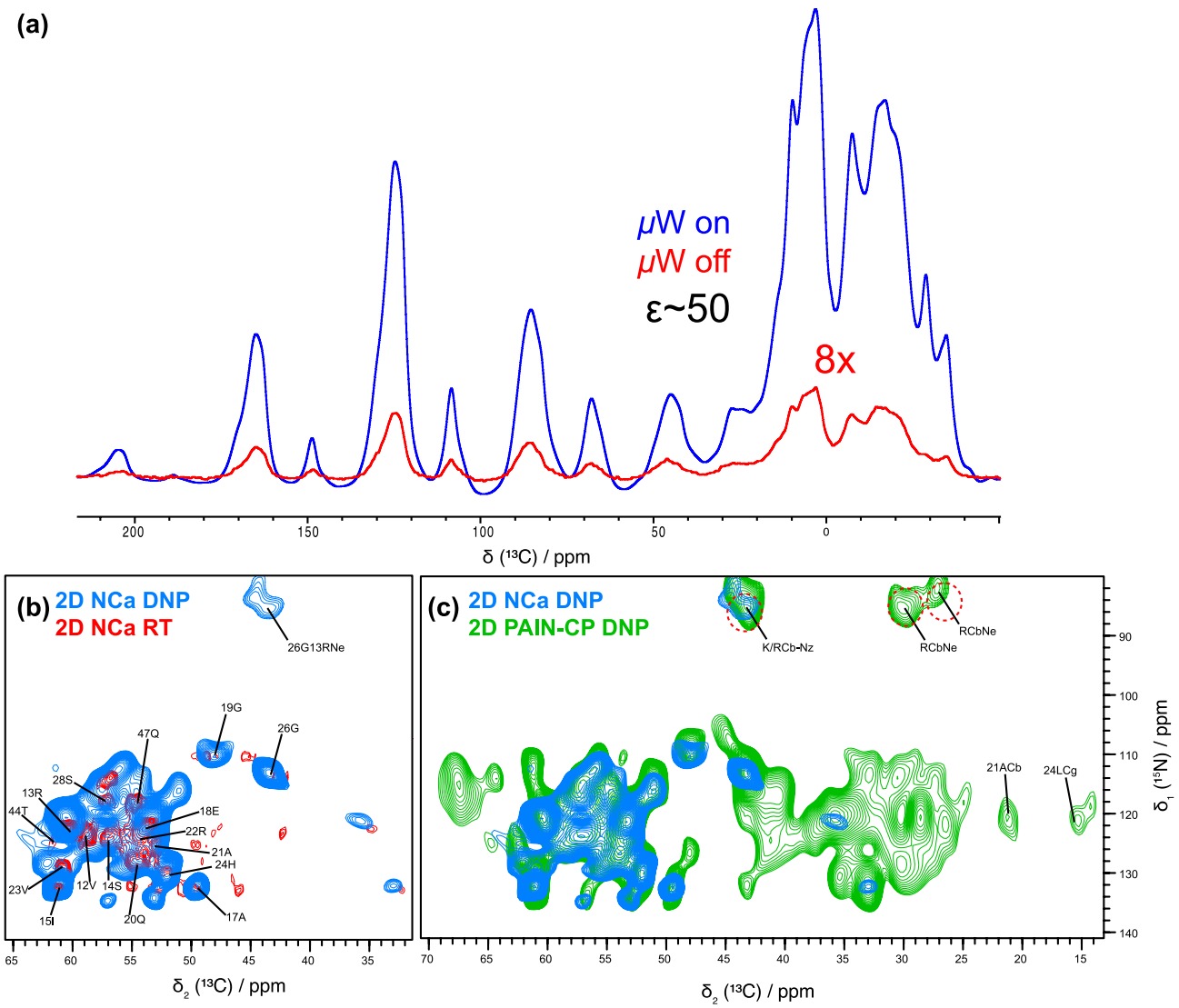

Fig. 3 **a** Comparison of 1D ^{1}H–^{13}C CP spectra of NWD2 amyloid fibrils with 5 mM SNAPol-1 recorded at 8 kHz MAS with microwave on (blue) and off (red) condition. Enhancement factor of ε ~ 50 was measured. **b** 2D NCa spectrum recorded with DNP at 100 K and 8.1 kHz MAS (blue), overlayed with a similar experiment acquired at 273 K and 11 kHz MAS (red). Both spectra were recorded at 18.8 T. **c** DNP-enhanced ^{15}N–^{13}C PAIN-CP (green) show long-range cross peaks that are absent in DNP NCa experiments (blue). The arginine and lysine peaks are not unambiguously assigned.

et al. 2017; Björklund et al. 2013; Maus et al. 1996), which unsurprisingly interferes with the ~ kHz rf fields and MAS frequencies employed in solid-state NMR experiments. Hence, when frozen at low temperatures, the side chains are sufficiently rigid to allow efficient polarization transfer through dipolar couplings—they become observable in CP-based ssNMR experiments.

To ease the assignment process of these newly observed peaks and obtain new distance restraints, we set up a 2D ^{15}N–^{13}C PAIN-CP experiment (Lewandowski et al. 2007; De Paëpe et al. 2011), which has been demonstrated to be efficient for obtaining the long-range heteronuclear distance restraints necessary for structure determination (Debelouchina et al. 2013; Melckebeke et al. 2010; Colvin et al. 2016; Loquet et al. 2012). Nevertheless, it is known that setting up PAR/PAIN-CP experiments is challenging due to the sensitive matching conditions, i.e., the radiofrequency (rf) nutation frequencies applied on the ^{1}H and ^{13}C for PAR (and additionally on the ^{15}N for PAIN-CP) have to be precisely configured for optimum performances (Lewandowski et al. 2007; Donovan et al. 2017a, 2017b). Hence, it is common to first optimize the PAR/PAIN-CP conditions on ^{13}C/^{15}N-labeled small peptides or model proteins before repeating the experiments on the larger and less sensitive target biomolecules. Such an optimization strategy is not ideal because the experimental parameters might be significantly

different in non-crystalline proteins such as hydrated protein assemblies, where the sample heterogeneity, rf inhomogeneity, and larger chemical shift dispersion might impede the PAR/PAIN transfer efficiency.

While it is possible to optimize the PAR/PAIN-CP condition directly on the interested proteins with a 1D spectrum, it is difficult to assess the efficiency of long-range transfers that is usually weaker and difficult to observe under the presence of stronger but less important short-range contacts. Hence, it is easier to find a robust matching condition with a 2D experiment, despite being more time-consuming. Thanks to the sensitivity enhancement of $\varepsilon \sim 50$ bestowed by DNP, we can acquire a ^{15}N–^{13}C PAIN-CP spectrum (Fig. 3c) with a modest signal-to-noise ratio in only two hours. To our knowledge, a DNP-enhanced PAIN spectrum has not been demonstrated in the literature. This could be because the relatively low biradical concentration (5 mM) used here, compared to the ≥ 10 mM biradical concentration employed in the literature (Sauvée et al. 2013; Fricke et al. 2016), leads to longer spin-locked relaxation times, $T_{1\rho}$, and hence more efficient PAR/PAIN-CP transfer (Corzilius et al. 2014). The resulting 2D ^{15}N–^{13}C PAIN-CP spectrum (Fig. 3c) shows numerous intra-residue correlations between backbone ^{15}N nuclei and the side chain ^{13}C nuclei. These signals are crucial to establish the amino-acid spin-system identification and correlating the signals observed in 2D ^{13}C–^{13}C experiments to those observed in the conventional 2D NCa experiment. In addition to ^{15}N backbone correlations, the frozen temperature conditions under DNP boost ^{15}N signals arising from side-chain nitrogen, typically from Nε of Arginine and/or Nζ from lysine (Fig. 3c). These residues have long side chains that keep an important mobility at room temperature, whose NMR signals can be uncovered by low-temperature DNP experiments. Note that similar correlations have also been observed for frequency-selective TEDOR experiments for bacteriorhodopsin using DNP (Bajaj et al. 2010).

Experimental section

Sample preparation

The ^{13}C–^{15}N labelled HETs(218–289), and NWD2 samples were prepared according to previously published protocols (Siemer et al. 2005). Both samples were mixed with either 5 mM M-TinyPol (CortecNet) or 5 mM SNAPol-1 radicals in DNP juice (d_8-glycerol: D_2O: H_2O in a ratio of 6:3:1 by volume) and incubated for 1 h at room temperature (RT). The samples were shortly centrifuged in a benchtop centrifuge ($\leq 2000\times g$) before being packed into sapphire rotors. We have used Vespel MAS drive caps instead of the vendor-recommended ZrO_2 drive caps because the latter design has a segmented insert, which can be easily damaged if mishandled. Nevertheless, the Vespel drive caps become loose at low temperatures due to a different heat expansion coefficient from the sapphire material. Hence, we marked the inserts of the Vespel caps with a permanent marker (Sharpie) to improve the seal between the rotor and the drive cap. The DNP sample was then degassed with at least three freeze–pump–thaw cycles using a 3-way tap, and backfilled with Argon gas (Delage-Laurin et al. 2021; Tan et al. 2022). This procedure removes the paramagnetic oxygen, which reproducibly improves the DNP enhancement factor by ~ 10%. We could not implement the insert/eject cycle degassing method demonstrated in Kubicki et al. because the rotor is likely to be blocked in our Bruker MAS DNP probe at lower temperatures (Kubicki et al. 2014).

DNP NMR spectroscopy

The spectra were acquired on a Bruker 800 MHz spectrometer, with a wide-bore 18.8 T magnet equipped with a 3.2 mm HCN DNP probe at the temperature T = 100 K and at 8–10 kHz MAS frequencies. Note that the M-TinyPol and SNAPol-1 samples coincidentally yield the maximum positive cross-effect DNP performances at the same static magnetic field B_0 for a fixed gyrotron microwave frequency. Hence, all DNP experiments were recorded at $B_0 = 18.796$ T (^1H Larmor frequency of 800.28 MHz) with a gyrotron microwave frequency of 526.965 ± 0.01 GHz. The gyrotron output power of 15 W (with 130 mA collector current in the gyrotron) was used in all DNP experiments. Although the commercial probe is rated for operation at ~ 10–12 kHz at ~ 100 K, we have performed most DNP experiments at 8 kHz MAS frequency, which is significantly less likely to have rotor crash events than the experiments at 10 kHz. The spectra were processed with TopSpin 3.1 (QSine = 3 apodization functions were applied for both dimensions in all 2D spectra) and analyzed with the CcpNmr 2.1 program (Vranken et al. 2005).

Conclusions

In summary, we have demonstrated the potential of DNP-MAS NMR in studying amyloid fibrils, particularly the semi-rigid protein segments and mobile side chains that are otherwise inaccessible in conventional room-temperature ssNMR experiments. We have obtained an enhancement factor of $\varepsilon \sim 50$ using SNAPol-1, which is the highest enhancement reported so far at 18.8 T for amyloid fibrils. Contrary to DNP studies reported on biomolecules, the ^{13}C nuclei in HET-s(218–289) fibrils retain a modest NMR resolution at cryogenic temperatures ($T \sim 100$ K) in DNP experiments. The boost of sensitivity and the low-temperature environment helps elucidate new peaks usually unobservable at

room temperature due to mobility in an unfavorable regime. Additionally, we demonstrated that a 2D ^{15}N-^{13}C PAIN-CP spectrum with excellent sensitivity could be obtained in less than 2 h. This approach allowed us to observe new correlations involving ^{15}N side chain nuclei. The promising DNP experiments and results will be combined with selective labelling schemes to obtain unambiguous distance restraints of previously unassigned peaks in the future. This will be crucial for refining the 3D structures of biological macromolecules and gaining insights into important biological functions.

Supplementary Information The online version contains supplementary material available at https://doi.org/10.1007/s10858-023-00416-5.

Acknowledgements A. Loquet acknowledges financial support from the European Research Council (ERC) under the European Unions Horizon 2020 research and innovation program (ERC-2015-StG GA No. 639020). A. Lends was supported by the Swiss National Science Foundation for the early postdoc mobility project (P2EZP2_184258). K.O.T is grateful for the fundings granted by the French National Research Agency: *PulsedDNP* (ANR-20-ERC9-0008) and *HFPulsedDNP* (ANR-21-CE29-0019). Financial support from the IR INFRANALYTICS FR2054 for conducting the research is gratefully acknowledged. Y.P.L. acknowledges the support from the National Natural Science Foundation of China (Nos. 22174099 and 21871210) and Science & Technology Projects of Tianjin (No. 20JCZDJC00050).

Author contributions A. Lends, A. Loquet, and KOT designed the research. The NMR samples were prepared in Bordeaux, while the DNP experiments were performed at ENS. XC and YPL provided the radicals. A. Lends wrote the first draft of the manuscript. All authors prepared the figures, edited, and reviewed the manuscript.

Funding Funding was provided by European Research Council (639020), Schweizerischer Nationalfonds zur Förderung der Wissenschaftlichen Forschung (P2EZP2_184258), Agence Nationale de la Recherche (ANR-20-ERC9-0008), National Natural Science Foundation of China (22174099), and Tianjin Science and Technology Program (20JCZDJC00050).

Declarations

Conflict of interest The authors declare that they have no conflict of interest.

References

Akbey Ü, Linden AH, Oschkinat H (2012) High-temperature dynamic nuclear polarization enhanced magic-angle-spinning NMR. Appl Magn Reson 43:81–90

Bahri S et al (2022) H detection and dynamic nuclear polarization—enhanced NMR of Aβ 1–42 fibrils.

Bajaj VS, Mak-Jurkauskas ML, Belenky M, Herzfeld J, Griffin RG (2010) DNP enhanced frequency-selective TEDOR experiments in bacteriorhodopsin. J Magn Reson 202:9–13

Barnes AB et al (2009) Cryogenic sample exchange NMR probe for magic angle spinning dynamic nuclear polarization. J Magn Reson 198:261–270

Barnes AB et al (2010) Resolution and polarization distribution in cryogenic DNP/MAS experiments. Phys Chem Chem Phys 12:5861

Bauer T et al (2017) Line-broadening in low-temperature solid-State NMR spectra of fibrils. J Biomol NMR 67:51–61

Bayro MJ et al (2011) Intermolecular structure determination of amyloid fibrils with magic-angle spinning and dynamic nuclear polarization NMR. J Am Chem Soc 133:13967–13974

Berruyer P (2020) Dynamic nuclear polarization enhancement of 200 at 21.15 T enabled by 65 kHz magic angle spinning. J Phys Chem Lett 11:8386–8391.

Biedenbänder T, Aladin V, Saeidpour S, Corzilius B (2022) Dynamic nuclear polarization for sensitivity enhancement in NMR. Chem Rev.

Björklund S, Nowacka A, Bouwstra JA, Sparr E, Topgaard D (2013) Characterization of stratum corneum molecular dynamics by natural-abundance 13C solid-state NMR. PLoS ONE.

Blank M, Borchard P, Cauffman S, Felch K, Rosay M (2016) Development of high-frequency cw gyrotrons for DNP/NMR applications. Terahertz Sci Technol 9:177–186

Cai X et al (2021) Highly efficient trityl-nitroxide biradicals for biomolecular high-field dynamic nuclear polarization. Chemisty A 27:12758–12762

Chapman MR et al (2002) Role of *Escherichia coli* curli operons in directing amyloid fiber formation. Science (80-) 295:851–855

Colvin MT et al (2015) High resolution structural characterization of Aβ42 amyloid fibrils by magic angle spinning NMR. J Am Chem Soc 137:7509–7518

Colvin MT et al (2016) Atomic resolution structure of monomorphic Aβ 42 amyloid fibrils. J Am Chem Soc 138:9663–9674

Conroy DW et al (2022) Probing Watson-Crick and Hoogsteen base pairing in duplex DNA using dynamic nuclear polarization solid-state NMR spectroscopy. Proc Natl Acad Sci USA

Corzilius B, Andreas LB, Smith AA, Ni QZ, Griffin RG (2014) Paramagnet induced signal quenching in MAS-DNP experiments in frozen homogeneous solutions. J Magn Reson 240:113–123

Daskalov A et al (2015) Signal transduction by a fungal NOD-like receptor based on propagation of a prion amyloid fold. PLoS Biol 13:1–26

Daskalov A et al (2020) Structural and molecular basis of cross-seeding barriers in amyloids. Proc Natl Acad Sci USA 118:1–8

Daskalov A et al (2021) Structures of pathological and functional amyloids and prions, a solid-state NMR perspective. Front Mol Neurosci 14:1–18

David G et al (2018) Structural studies of self-assembled subviral particles: combining cell-free expression with 110 kHz MAS NMR spectroscopy. Angew Chem Int Ed 57:4787–4791

De Paëpe G et al (2011) Heteronuclear proton assisted recoupling. J Chem Phys 134:1–18

Debelouchina GT et al (2013) Higher order amyloid fibril structure by MAS NMR and DNP spectroscopy. J Am Chem Soc 135:19237–19247

Delage-Laurin L et al (2021) Overhauser dynamic nuclear polarization with selectively deuterated BDPA radicals. J Am Chem Soc 143:20281–20290

Deo T, Cheng Q, Paul S, Qiang W, Potapov A (2021) Application of DNP-enhanced solid-state NMR to studies of amyloid-β peptide interaction with lipid membranes. Chem Phys Lipids 236:105071

Dobson CM, Knowles TPJ, Vendruscolo M (2020) The amyloid phenomenon and its significance in biology and medicine. Cold Spring Harb Perspect Biol 12

Donovan KJ, Jain SK, Silvers R, Linse S, Griffin RG (2017a) Proton-assisted recoupling (PAR) in peptides and proteins. J Phys Chem B 121:10804–10817

Donovan KJ, Silvers R, Linse S, Griffin RG (2017b) 3D MAS NMR experiment utilizing through-space 15 N– 15 N correlations. J Am Chem Soc 139:6518–6521

Felch K et al (2013) First tests of a 527 GHz gyrotron for dynamic nuclear polarization. In 2013 IEEE 14th international vacuum electronics conference (IVEC) 1–2 (IEEE, 2013).
Fitzpatrick AWP et al (2013) Atomic structure and hierarchical assembly of a cross-β amyloid fibril. Proc Natl Acad Sci USA 110:5468–5473
Fitzpatrick AW, Saibil HR (2019) Cryo-EM of amyloid fibrils and cellular aggregates. Curr Opin Struct Biol 58:34–42
Frederick KK et al (2017) Combining DNP NMR with segmental and specific labeling to study a yeast prion protein strain that is not parallel in-register. Proc Natl Acad Sci USA 114:3642–3647
Fricke P, Demers JP, Becker S, Lange A (2014) Studies on the MxiH protein in T3SS needles using DNP-enhanced ssNMR spectroscopy. ChemPhysChem 15:57–60
Fricke P et al (2016) High resolution observed in 800 MHz DNP spectra of extremely rigid type III secretion needles. J Biomol NMR 65:121–126
Gath J et al (2014) Yet another polymorph of α-synuclein: solid-state sequential assignments. Biomol NMR Assign 8:395–404
Gauto DF et al (2019) Aromatic ring dynamics, thermal activation, and transient conformations of a 468 kDa enzyme by specific 1H–13C labeling and fast magic-angle spinning NMR. J Am Chem Soc 141:11183–11195
Gauto D, Dakhlaoui O, Marin-Montesinos I, Hediger S, De Paëpe G (2021) Targeted DNP for biomolecular solid-state NMR. Chem Sci 12:6223–6237
Halbritter T, Harrabi R, Paul S, Tol JV, Lee D, Sigurdsson ST, Mentink-Vigier F, De Paëpe G (2022) PyrroTriPol: a Semi-rigid trityl-nitroxide for high field dynamic nuclear polarization. Chem. Sci.
Heise H et al (2008) Solid-state NMR reveals structural differences between fibrils of wild-type and disease-related A53T mutant α-synuclein. J Mol Biol 380:444–450
Henstra A, Dirksen P, Schmidt J, Wenckebach WT (1988) Nuclear spin orientation via electron spin locking (NOVEL). J Magn Reson 77:389–393
Jaroniec CP (2019) Two decades of progress in structural and dynamic studies of amyloids by solid-state NMR. J Magn Reson 306:42–47
Jaudzems K et al (2018) Dynamic nuclear polarization-enhanced biomolecular NMR spectroscopy at high magnetic field with fast magic-angle spinning. Angew Chem Int Ed 7458–7462.
Jaudzems K, Polenova T, Pintacuda G, Oschkinat H, Lesage A (2019) DNP NMR of biomolecular assemblies. J Struct Biol 206:90–98
Jirasko V et al (2021) Dimer organization of membrane-associated NS5A of hepatitis C virus as determined by highly sensitive 1H-detected solid-state NMR. Angew Chem Int Ed 60:5339–5347
Ke PC et al (2020) Half a century of amyloids: past, present and future. Chem Soc Rev 49:5473–5509
Kubicki DJ et al (2014) Amplifying dynamic nuclear polarization of frozen solutions by incorporating dielectric particles. J Am Chem Soc 136:15711–15718
Lewandowski JR, De Paëpe G, Griffin RG (2007) Proton assisted insensitive nuclei cross polarization. J Am Chem Soc 129:728–729
Li Y et al (2021) Solid-state MAS NMR at ultra low temperature of hydrated alanine doped with DNP radicals. J Magn Reson 333:107090
Lopez del Amo J-M, Schneider D, Loquet A, Lange A, Reif B (2013) Cryogenic solid state NMR studies of fibrils of the Alzheimer's disease amyloid-β peptide: perspectives for DNP. J Biomol NMR 56:359–363
Loquet A, Saupe SJ (2017) Diversity of amyloid motifs in NLR signaling in fungi. Biomolecules 7:1–10
Loquet A et al (2012) Atomic model of the type III secretion system needle. Nature 486:276–279
Loquet A, Saupe SJ, Romero D (2018a) Functional amyloids in health and disease. J Mol Biol 430:3629–3630
Loquet A et al (2018b) 3D structure determination of amyloid fibrils using solid-state NMR spectroscopy. Methods.
Lund A et al (2020) TinyPols: a family of water-soluble binitroxides tailored for dynamic nuclear polarization enhanced NMR spectroscopy at 18.8 and 21.1 T. Chem Sci 68:42–61.
Maciejko J et al (2015) Visualizing specific cross-protomer interactions in the homo-oligomeric membrane protein proteorhodopsin by dynamic-nuclear-polarization-enhanced solid-state NMR. J Am Chem Soc 137:9032–9043
Maji SK et al (2009) Functional amyloids as natural storage of peptide hormones in pituitary secretory granules. Science (80-) 325:328–332
Marin-Montesinos I et al (2019) Selective high-resolution DNP-enhanced NMR of biomolecular binding sites. Chem Sci 10:3366–3374
Mathies G et al (2015) Efficient dynamic nuclear polarization at 800 MHz/527 GHz with trityl-nitroxide biradicals. Angew Chemie - Int Ed 54:11770–11774
Matsuki Y, Idehara T, Fukazawa J, Fujiwara T (2016) Advanced instrumentation for DNP-enhanced MAS NMR for higher magnetic fields and lower temperatures. J Magn Reson 264:107–115
Maus DC et al (1996) A solid-state NMR study of tungsten methyl group dynamics in [W(η 5-C 5Me 5)Me 4][PF 6]. J Am Chem Soc 118:5665–5671
Meier BH, Böckmann A (2015) The structure of fibrils from 'misfolded' proteins. Curr Opin Struct Biol 30:43–49
Menzildjian G et al (2021) Efficient dynamic nuclear polarization up to 230 K with hybrid BDPA-nitroxide radicals at a high magnetic field. J Phys Chem B 125:13329–13338
Nagaraj M et al (2016) Surface binding of TOTAPOL assists structural investigations of amyloid fibrils by dynamic nuclear polarization NMR spectroscopy. ChemBioChem.
Ni QZ et al (2017) Peptide and protein dynamics and low-temperature/DNP magic angle spinning NMR. J Phys Chem B (2017). https://doi.org/10.1021/acs.jpcb.7b02066
Potapov A, Yau W, Ghirlando R, Thurber KR, Tycko R (2015) Successive stages of amyloid-β self-assembly characterized by solid-state nuclear magnetic resonance with dynamic nuclear polarization. J Am Chem Soc 137:8294–8307
Purea A et al (2019) Improved waveguide coupling for 1.3mm MAS DNP probes at 263 GHz. J Magn Reson 302:43–49
Rankin A, Trébosc J, Pourpoint F, Amoureux J-P, Lafon O (2019) Recent developments in MAS DNP-NMR of materials. Solid State Nucl Magn Reson.
Ravotti F et al (2016) Solid-state NMR sequential assignment of an Amyloid-β(1–42) fibril polymorph. Biomol NMR Assign 10:269–276
Redrouthu VS, Mathies G (2022) Efficient pulsed dynamic nuclear polarization with the X-Inverse-X sequence. J Am Chem Soc 144:1513–1516
Sauvée C et al (2013) Highly efficient, water-soluble polarizing agents for dynamic nuclear polarization at high frequency. Angew Chem 52:10858–10861
Sesti EL et al (2018) Magic angle spinning NMR below 6 K with a computational fluid dynamics analysis of fluid flow and temperature gradients. J Magn Reson 286:1–9
Siemer AB (2020) Advances in studying protein disorder with solid-state NMR. Solid State Nucl Magn Reson 106:101643
Siemer AB, Ritter C, Ernst M, Riek R, Meier BH (2005) High-resolution solid-state NMR spectroscopy of the prion protein HET-s in its amyloid conformation. Angew Chem 44:2441–2444
Siemer AB et al (2006) Observation of highly flexible residues in amyloid fibrils of the HET-s prion. J Am Chem Soc 128:13224–13228

Su Y, Andreas L, Griffin RG (2015) Magic angle spinning NMR of proteins: high-frequency dynamic nuclear polarization and (1)H detection. Annu Rev Biochem 84:465–497

Takahashi H, Hediger S, De Paëpe G (2013) Matrix-free dynamic nuclear polarization enables solid-state NMR 13C–13C correlation spectroscopy of proteins at natural isotopic abundance. Chem Commun 49:9479–9481

Tan KO, Jawla S, Temkin RJ, Griffin RG (2019a) Pulsed dynamic nuclear polarization. eMagRes 339–352.

Tan KO, Yang C, Weber RT, Mathies G, Griffin RG (2019b) Time-optimized pulsed dynamic nuclear polarization. Sci Adv 5:eaav6909

Tan KO et al (2022) Observing nearby nuclei on paramagnetic trityls and MOFs via DNP and electron decoupling. Chem. Eur. J.

Thankamony AS, Wittmann JJ, Kaushik M, Corzilius B (2017) Dynamic nuclear polarization for sensitivity enhancement in modern solid-state NMR. Prog Nucl Magn Reson Spectrosc 102–103:120–195

Thurber K, Tycko R (2016) Low-temperature dynamic nuclear polarization with helium-cooled samples and nitrogen-driven magic-angle spinning. J Magn Reson 264:99–106

Thurber K, Yau W, Tycko R (2010) Low-temperature dynamic nuclear polarization at 9.4 T with a 30 mW microwave source. J Magn Reson 204:303–313

Tycko R (2014) Physical and structural basis for polymorphism in amyloid fibrils. Protein Sci 23:1528–1539

van der Wel PCA (2017) Insights into protein misfolding and aggregation enabled by solid-state NMR spectroscopy. Solid State Nucl Magn Reson 88:1–14

Van Melckebeke H et al (2010) Atomic-resolution three-dimensional structure of HET-s(218–289) amyloid fibrils by solid-state NMR spectroscopy. J Am Chem Soc 132:13765–13775

Van Melckebeke H et al (2011) Probing water accessibility in HET-s(218–289) amyloid fibrils by solid-state NMR. J Mol Biol 405:765–772

Vranken WF et al (2005) The CCPN data model for NMR spectroscopy: development of a software pipeline. Proteins Struct Funct Genet 59:687–696

Wasmer C et al (2008) Amyloid fibrils of the HET-s(218–289) prion form a beta solenoid with a triangular hydrophobic core. Science 319:1523–1526

Wiegand T et al (2016) Solid-state NMR sequential assignments of the N-terminal domain of HpDnaB helicase. Biomol NMR Assign 10:13–23

Wili N et al (2022) Designing broadband pulsed dynamic nuclear polarization sequences in static solids. Sci Adv 8:1–13

Wisser D et al (2018) BDPA-nitroxide biradicals tailored for efficient dynamic nuclear polarization enhanced solid-state NMR at magnetic fields up to 21.1 T. J Am Chem Soc 140:13340–13349

Zhai W et al (2020) Postmodification via thiol-click chemistry yields hydrophilic trityl-nitroxide biradicals for biomolecular high-field dynamic nuclear polarization. J Phys Chem B 124:9047–9060

Zhao W, Fernando LD, Kirui A, Deligey F, Wang T (2020) Solid-state NMR of plant and fungal cell walls: a critical review. Solid State Nucl Magn Reson 107:101660